Journal of Alloys and Compounds 509 (2011) 10098–10104

Contents lists available at ScienceDirect

Journal of Alloys and Compounds

journal homepage: www.elsevier.com/locate/jallcom

Microstructure morphologies during the transient solidification of hypomonotectic and monotectic Al–Pb alloys

Adrina P. Silva[a], Amauri Garcia[a], José E. Spinelli[b,*]

[a] Department of Materials Engineering, University of Campinas–UNICAMP, PO Box 6122 – 13083-970 – Campinas, SP, Brazil
[b] Department of Materials Engineering, Federal University of São Carlos – UFSCar, 13565-905, São Carlos, SP, Brazil

ARTICLE INFO

Article history:
Received 24 June 2011
Accepted 10 August 2011
Available online 19 August 2011

Keywords:
Solidification
Monotectics
Microstructure
Solidification thermal parameters
Interphase spacing

ABSTRACT

The solidification cooling rate (T), growth rate (v), temperature gradient (G), interphase spacing (λ) and diameter (d) of the Pb-rich phase have been experimentally determined for a hypomonotectic Al–0.9 wt%Pb and a monotectic Al–1.2 wt%Pb alloys directionally solidified under unsteady-state heat flow conditions. It is shown for both cases that, from the cooled bottom of the casting up to a certain position along the casting length, the microstructure was characterized by well-dispersed Pb-rich droplets in the aluminum-rich matrix, followed by a region of morphological transition (with the Pb-rich phase formed by droplets and fibers) and finally by a mixture of fibers and strings of pearls for positions closer to the top of the casting. It has been also observed that such microstructural transition was anticipated for the alloy with higher solute content. It is shown that the correlation between the morphology of the Pb-rich phase and the growth rate can be synthesized as follows: Al–0.9 wt%Pb alloy, droplets for $v > 1.0$ mm/s and fibers for $v < 0.65$ mm/s; Al–1.2 wt%Pb alloy, droplets for $v > 1.1$ mm/s and fibers for $v < 0.87$ mm/s. Experimental growth laws relating the interphase spacing to both G and v are proposed.
© 2011 Elsevier B.V. All rights reserved.

1. Introduction

Monotectic binary alloys are characterized by limited mutual component solubility in the liquid state. The monotectic reaction occurs when a liquid of composition L_1, at the monotectic temperature, decomposes into a solid phase α and another liquid phase L_2. Some of these alloys are of special technical importance as, for instance, electrical power switches (Ni–Ag) or self-lubricated bearings (Al–Pb and Al–Bi) [1–4].

In most monotectic systems the solid phase α forms a continuous matrix whereas the liquid phase L_2 is discontinuous, being retained in isolated pockets within the solid matrix. The comprehension of microstructure formation during casting of monotectic alloys is fundamental for the design of suitable tribological properties. Al–Pb alloys are especially indicated as advanced bearing materials due to their combination of abundant availability, high strength to weight ratio and excellent friction and wear properties [5]. Johnson et al. [6] stated that the monotectic alloys are difficult to be manufactured by conventional processing due to the extent of the miscibility gap. These authors affirm that alloys with relatively homogeneous microstructures of fine Pb particles in an Al matrix could be made by metastable processing such as rapid solidification, ion implantation, ball milling and physical vapor deposition. A comprehensive study on the mechanisms governing the formation of shell-type structure in the powder surface of atomized Al–30 wt%Pb drops was performed by Zhao [7]. Powders with shell-type structures have great potential for industrial application. One example is the development of the solder ball for modern electronic packaging technology. The author stated that the formation of the minor phase shell on the surface of the hypermonotectic Al–30 wt%Pb alloy powders is due to the heterogeneous nucleation of the minor phase droplets on the surface of the atomized drop and the resultant diffusional transfer of solute during the liquid–liquid phase transformation.

Monotectics are also described as composite materials having particles, rods or filaments of one metal or compound dispersed within a matrix of another [8]. Previous studies have been concerned with the control of the distribution of rods or spheres of the minor constituent in the solvent-rich matrix. Some tested methods are: addition of dopant elements such as iron [8], melt spinning [9], magnetic field [10] and solidification under microgravity [11–13].

Solidification of melts under microgravity appears to be a suitable method since convection and gravity induced segregation can be neglected. Ozawa and Motegi [13] investigated the influence of microgravity on the solidified microstructure of hypermonotectic Al–Pb alloys. Despite the lower cooling rate under microgravity cooling conditions compared with that exhibited under normal gravity, it was found that the microstructure of the samples con-

* Corresponding author. Tel.: +55 16 33 51 85 12; fax: +55 16 33 61 54 04.
E-mail address: spinelli@ufscar.br (J.E. Spinelli).

0925-8388/$ – see front matter © 2011 Elsevier B.V. All rights reserved.
doi:10.1016/j.jallcom.2011.08.049

sisted of a rather homogeneous distribution of lead particles. The use of dopants is a traditional method capable of breaking down the liquid–solid interface for the chosen alloy into a cellular pattern upon directional solidification from the melt [8]. The severity of gravity segregation in hypermonotectic Al–Pb alloys seems to be reduced during processing by melt spinning. Suh and Lee [9] stated that a more homogeneous solute distribution can be obtained for undercooling lower than 3 K. Magnetic field is also an interesting method to homogenise the distribution of Pb particles. According to Li and Zhao [10], the application of a static magnetic field during directional solidification can minimize the convective effects. This can cause a more uniform distribution of the nucleation rate of the minority phase as well as a decrease in the maximum size of the droplets in front of the solidification interface. Thus, a well-dispersed microstructure can be obtained.

Kaukler et al. [14] developed an X-ray transmission microscope (XTM) for studies of horizontal directional solidification of monotectic alloys under steady-state conditions. They found microstructural transitions during the tests with a hypermonotectic Al–1.5 wt%Pb, which were related to the imposed pulling rates. Monodisperse distribution of spherical Pb particles was found for pulling rates exceeding 6.0 μm/s. Fibers and strings of pearls were noted for lower velocities.

It is essential stress that the morphology of soft phase in monotectic alloys is also a feature to be controlled during processing. Microstructural transition in a monotectic Al–Bi alloy has been recently reported by Ratke and Müller [15,16]. They observed the bismuth-phase arranged as both fibers and strings of pearls after performing directional solidification experiments under steady-state heat flow conditions. Although the Jackson–Hunt model [17] was developed for eutectic growth, some authors [15,18–20] state that this classical relation $\lambda^2 v = C$ (λ is interphase spacing, v is growth rate and C is a constant) may be also valid to the fibrous monotectic growth. On the other hand, proper models have to be developed in order to describe the monotectic growth concerning both string of pearls and droplets.

Some factors affect significantly the microstructure evolution of monotectic alloys, namely: the temperature gradient (G), solidification velocity (v), concentration gradient, melt flow and natural convection [10]. In particular, microstructural features such as the interphase spacing (λ) and the relation between the diameter and the width (d/w) of the Pb-rich particles should be correlated to the aforementioned factors. The establishment of correlations between these microstructural features and solidification thermal parameters (G and v) can be useful in order to pre-programming the manufacturing casting processes. The focus is to produce components with a compromise between microstructural arrangement and good mechanical properties. Nevertheless, experimental reports on the microstructural evolution of monotectic Al–Pb alloys are scarce in literature.

The majority of the aforementioned studies existing in the literature have used Bridgman-type furnaces to produce the directionally solidified monotectic samples. The data obtained for stationary conditions do not reached a sufficient span of solidification velocities. This limitation can be overcome with the use of water-cooled experimental setups, which permit not only transient heat flow conditions during directional solidification (which are of prime importance since this class of heat flow encompasses the majority of solidification industrial processes) but also a larger spectrum of solidification velocities.

Directionally solidified hypomonotectic Al–0.9 wt%Pb and monotectic Al–1.2 wt%Pb alloys have been examined in the present study. The experimental setup permitted solidification under nonsteady-state freezing conditions as well as a wide range of solidification conditions to be examined. The present article was planned with a view to investigating both the microstructural evolution of the minority phase and the dependence of interphase spacing, size and morphology of the Pb-rich minority phase on the solidification thermal parameters and on the alloy solute content.

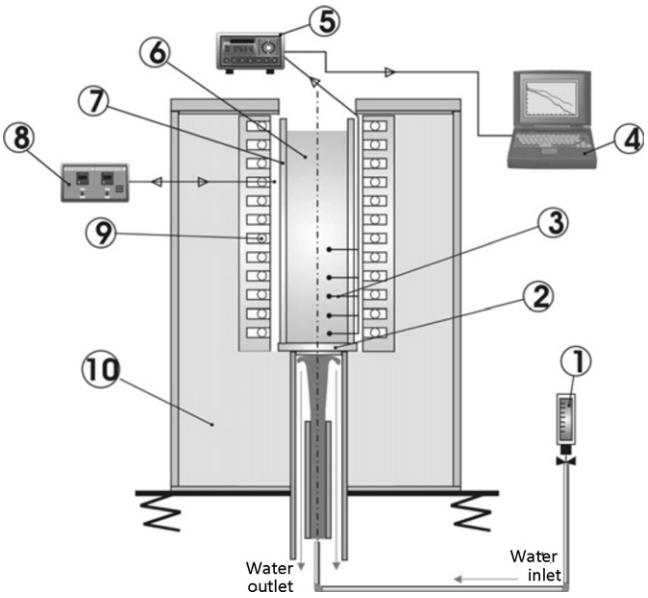

Fig. 1. Schematic representation of the experimental setup: (1) rotameter; (2) heat extracting bottom; (3) thermocouples; (4) computer and data acquisition software; (5) data logger; (6) casting; (7) mold; (8) temperature controller; (9) electric heaters; (10) insulating ceramic shielding.

2. Experimental procedure

The casting assembly used in solidification experiments is detailed in Fig. 1. Heat is directionally extracted only through a water-cooled bottom made of low carbon steel (SAE 1020), promoting vertical upward directional solidification. The experiment was performed with the Al–0.9 wt%Pb hypomonotectic and the monotectic Al–1.2 wt%Pb alloys, being the initial melt temperature (T_p) adjusted at 5% above the liquidus and monotectic temperatures, respectively. A detailed partial phase diagram of the Al–Pb system, calculated by the Thermo-Calc software, is shown in Fig. 2.

Continuous temperature measurements in the castings were monitored during solidification via the output of fine type K thermocouples (made from 0.2 mm

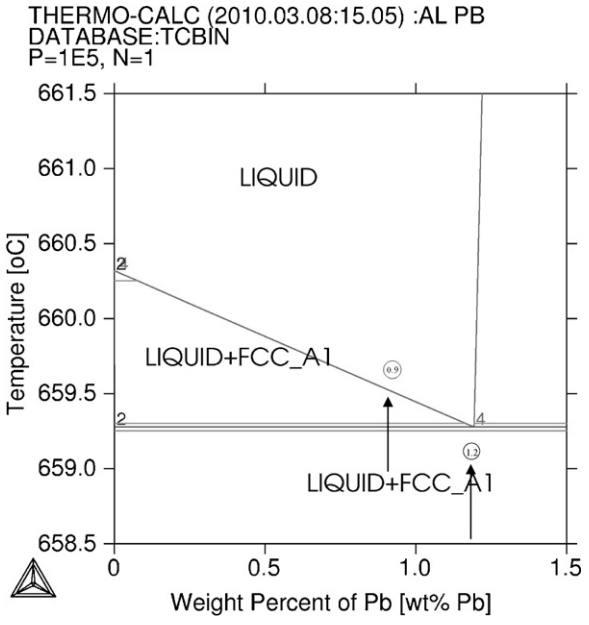

Fig. 2. Partial phase diagram of the Al–Pb system. The arrows indicate the Al–Pb chemistries examined in the present study.

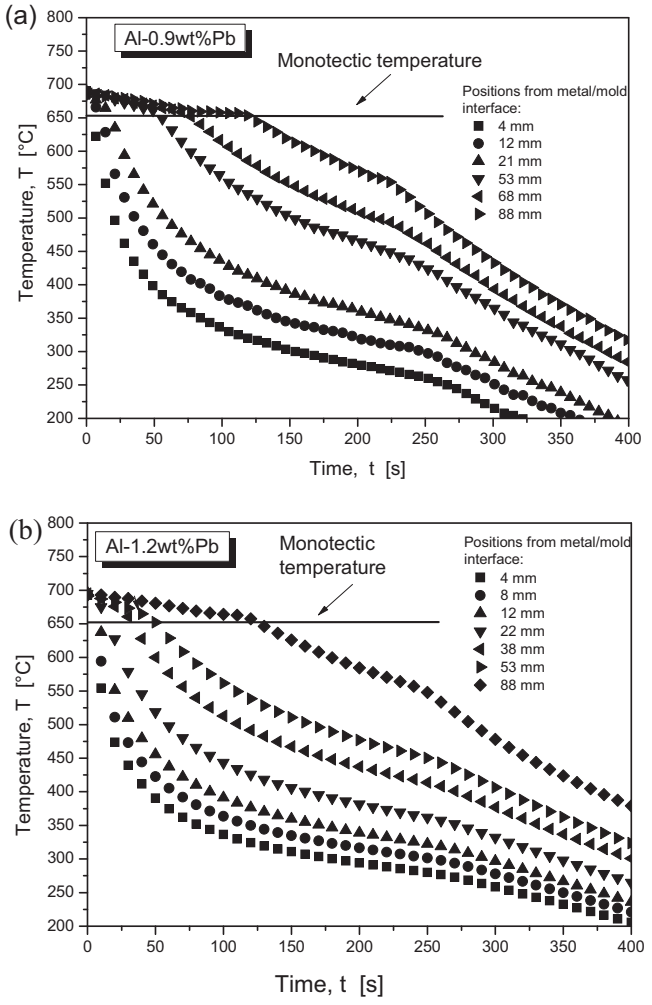

Fig. 3. Experimental cooling curves for thermocouples inside the castings: (a) Al–0.9 wt%Pb and (b) Al–1.2 wt%Pb.

diameter wire), which were placed at the positions 4, 8, 12, 21, 53, 68 and 88 mm from the cooled bottom of the casting. The thermocouples were calibrated at the melting point of aluminum exhibiting fluctuations of about 1 °C. All of the thermocouples were connected by coaxial cables to a data logger interfaced with a computer, and the temperature data, read at intervals of 0.1 s, were automatically acquired.

The cylindrical ingots were subsequently sectioned along its vertical axis, ground and etched with an acid solution to reveal the macrostructure (Poulton's reagent: 5 mL H_2O; 5 mL HF – 48%; 30 mL HNO_3; 60 mL HCl). Selected longitudinal sections (parallel to the growth direction) along the casting length were electropolished and etched (a solution of 0.5% HF in water) for metallography. Image processing systems were used to measure the interphase spacing, λ (about 50 independent readings for each selected position). The λ values were measured on the longitudinal section by averaging the horizontal distance between the Pb particles, adopting as reference the center of each particle. The size of the Pb-rich particles along the casting length was also measured.

3. Results and discussion

Fig. 3 depicts the resulting experimental cooling curves for the thermocouples inserted in the Al–0.9 wt%Pb and Al–1.2 wt%Pb alloys castings. The experimental thermal solidification parameters like growth rate (v), cooling rate ($\dot{T}$) and temperature gradient (G) can be determined from these temperature profiles.

The thermocouples readings have been used to generate a plot of position from the metal/mold interface as a function of time corresponding to either the monotectic front (Al–1.2 wt%Pb alloy) or the liquidus isotherm (Al–0.9 wt%Pb alloy) passing by each thermocouple. A curve fitting technique on these experimental points yielded a power function of position as a function of time. The derivative of these functions with respect to time gave values for both the monotectic growth velocity and the tip growth rate, v. Fig. 4a shows the experimental evolutions of v for the experimentally examined alloys. The experimental cooling rates (Fig. 4b) were then determined by considering the thermal data recorded immediately after the passing of either the monotectic front or the liquidus isotherm by each thermocouple. Temperature gradients (G) were determined from the experimental values of cooling rate and growth rate, i.e.: $G = \dot{T}/V$ (Fig. 4c).

Figs. 5 and 6 show typical macrostructures and microstructures obtained after metallographic examination. Columnar grains prevailed in the entire length of the solidified castings, which means that vertically aligned grains have grown from the bottom of the casting. In these figures, the chosen longitudinal microstructures (optical and SEM images) refer to three different positions in the casting from the cooled bottom. Such positions were chosen in order to evaluate the effect of the free change of solidification thermal variables along the casting length on the resulting microstructure. The water-cooled mold imposes higher values of cooling rates close to the bottom of the casting and a decreasing profile along the casting length due to the increasing thermal resistance of the solidified shell with increasing distance from the cooled bottom. This influence translates to the microstructural growth, with smaller interphase spacings at the bottom and larger ones close to the top of the casting.

In both cases the resulting microstructure close to the bottom of the casting is formed by Pb-rich droplets having diameters of about 3.5 and 3.2 μm for Al–0.9 wt%Pb and Al–1.2 wt%Pb alloys, respectively, dispersed in the Al-rich matrix. This microstructure prevails up to distances of about 20 mm and 15 mm from the casting cooled bottom for the Al–0.9 wt%Pb and Al–1.2 wt%Pb alloys, respectively. The range of coexistence of Pb-rich fibers and droplets is much larger in the case of the Al–0.9 wt%Pb alloy, remaining between 20 mm and 85 mm from the bottom of the casting, characterizing a region of transition of the microstructure morphology. The microstructural transition for the Al–1.2 wt%Pb alloy occurred from 15 mm to 30 mm from the bottom of the casting. After the transition region, Pb-rich fibers and strings of pearls are the predominant morphologies for positions >85 mm and >30 mm up to the top of the castings for the Al–0.9 wt%Pb and Al–1.2 wt%Pb alloys, respectively, as can be seen in Figs. 5 and 6.

Fig. 7 shows the microstructure evolution along the casting length. The experimental interphase spacing measured for both droplets and fibers as a function of position in the castings (distance from the bottom of the casting) is also depicted in Fig. 7.

Fig. 8a and b shows the mean experimental values of the interphase spacing measured from the aforementioned microstructures as a function of the growth rate, v. Points are experimental results and lines represent the empirical fit on the experimental points, with λ being expressed as a power function of the growth rate. It can be observed in Fig. 8a and b that the Pb-rich phase has a droplet morphology for $v > 1.0$ mm/s and $v > 1.1$ mm/s for Al–0.9 wt%Pb and Al–1.2 wt%Pb alloys, respectively. On the other hand, a fiber-like Pb-rich phase prevails for $v < 0.65$ mm/s and $v < 0.87$ mm/s for Al–0.9 wt%Pb and Al–1.2 wt%Pb alloys, respectively. According to Ratke [15,16] the competition between the growth of the minority phase and the advancement of the solidification front, will determine if fibers will prevail or irregularly arranged droplets will appear. If the rate of the solidification front is faster than the droplets growth, the droplets are engulfed by the advancing front. If the solidification front moves slower with respect to the droplets growth, fibers can be formed.

Ratke [11,12,15,16] states that when a monotectic alloy solidifies with a fibrous structure, it has the same functional dependence on growth rate as the interlamellar separation in eutectic alloys.

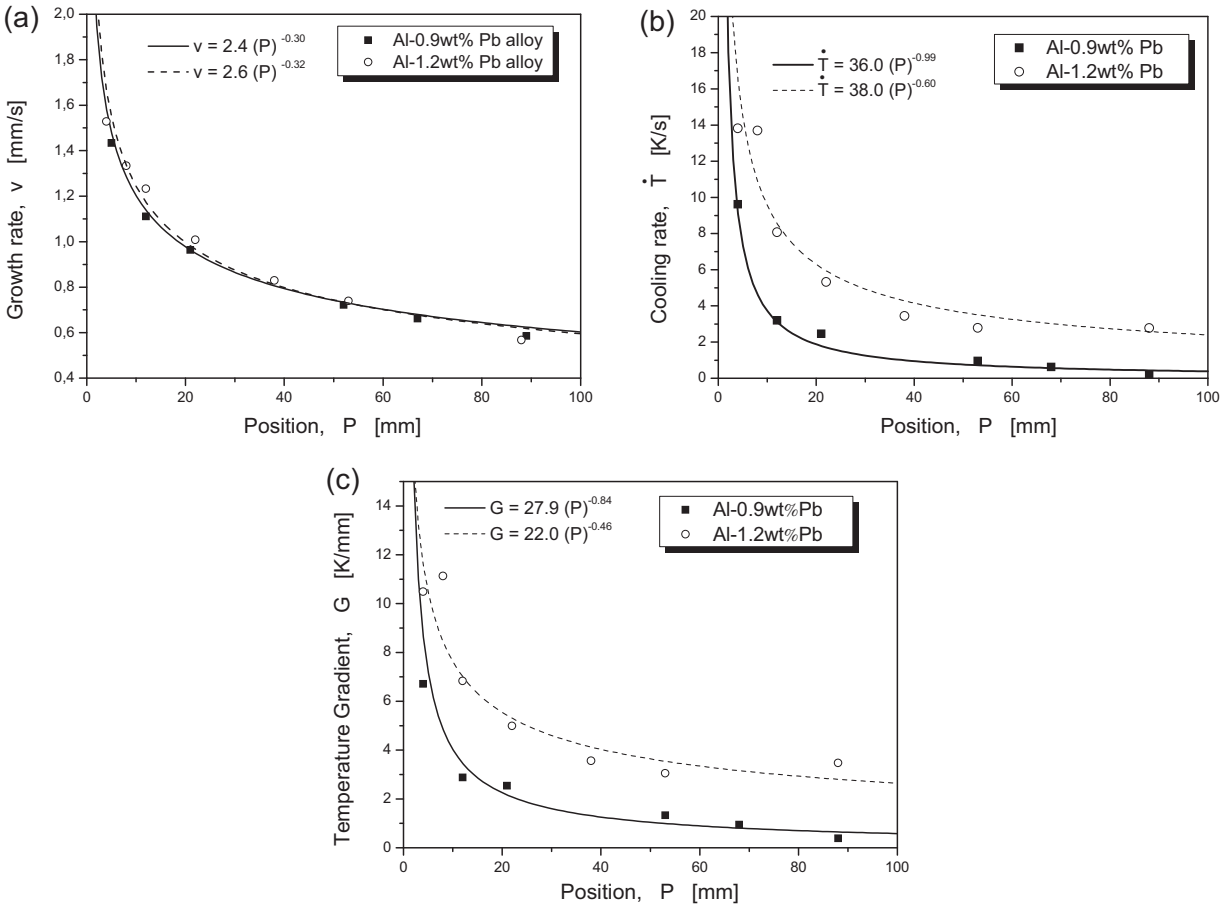

Fig. 4. (a) Growth rate; (b) cooling rate; (c) temperature gradient as a function of position from the cooled bottom of the casting during transient directional solidification.

On the other hand, appropriate models permitting the growth and distribution of droplets to be described, are still in development. The relationship proposed by Jackson and Hunt [17] is $\lambda^2 v = C$ (constant), which would be valid for the growth of fibrous monotectics and eutectics. Two different experimental power functions relating the interphase spacing with the growth rate have been derived from the present experimental results: $\lambda = 20(v)^{-0.5}$ and $\lambda = 25(v)^{-0.5}$ for droplets while the fibrous morphology was characterized by higher exponents: $\lambda = 17(v)^{-2.2}$ and $\lambda = 23(v)^{-2.2}$, for Al–0.9 wt%Pb and Al–1.2 wt%Pb alloys, respectively. It can be seen that the Jackson–Hunt relationship was not able to encompass the fibrous growth during the transient directional solidification of these alloys.

An average constant C of about 5.5×10^{-13} was found to fit the classical growth law $\lambda^2 v = C$ for the two alloys examined in the present study. Such value is higher than other C values reported in the literature for monotectic growth [15,16,18–20]. It can be explained as a consequence of much higher velocities imposed by the present experimental solidification setup. In a study of steady and non-steady state growth of monotectic alloys Grugel et al. [21] reported that the corresponding C values differ by one or two orders of magnitude, the non-steady examples examined being much coarser at any given growth rate.

According to Ratke [16], the stable morphology of the minority solid phase during monotectic growth of alloys with exact monotectic composition is the fiber-like. The fibrous growth is only stable for high gradients and low growth rates, considering steady-state heat flow conditions during solidification. Indeed, in the present study the existence of fibers and string of pearls was observed, after the region of morphological transition, for $v < 0.87$ mm/s and $v < 0.65$ mm/s for the Al–1.2 wt%Pb and Al–0.9 wt%Pb alloys, respectively (Fig. 8).

The experimental growth rate profiles observed for both alloys are quite similar as can be seen in Fig. 4a. However, as shown in Fig. 8, the beginning of the morphological transition from droplets to fibers occurs for a slightly higher velocity for the Al–1.2 wt%Pb alloy. Although the difference concerning the alloys solute contents is small, it can be seen that the increase in solute content anticipates the transition. Lang [22] stated that the fluidity of Al–Pb alloys is increased with the increase in solute content. The final morphology of the minority phase can be affected by such parameter, especially considering that the improved flow conditions ahead the solidification front, due to higher fluidity, may improve the coalescence of fibers provided that preferential formation conditions are established. Furthermore, in the vertical upward configuration of the solidification setup used in the present experiments, the phase L_2 (which is denser than L_1) can settle towards the solidification front. This can impose a richer Pb layer at the monotectic front during directional solidification of the Al–1.2 wt%Pb alloy when compared with that of the Al–0.9 wt%Pb alloy. This condition seems to favor the coalescence of fibers.

The experimental evolution of the diameter of Pb-rich droplets as a function of the growth rate is shown in Fig. 9 for the two alloys experimentally examined. A single power law is able to represent the droplet size distribution along the casting length for both alloys, with the droplet size having a functional dependence on v characterized by a -1.5 exponent. The same exponent was reported

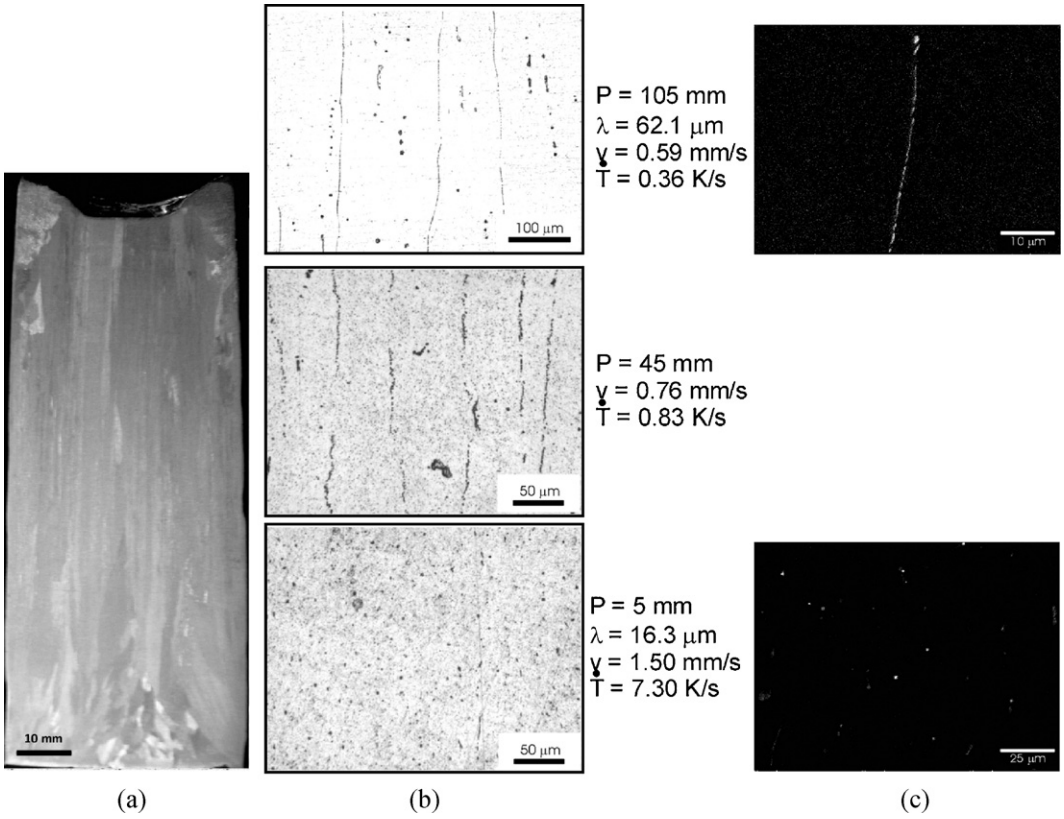

Fig. 5. (a) Directionally solidified macrostructure; (b) longitudinal microstructures and (c) microstructural details of the Pb-rich droplets and fibers (SEM images) of the Al–0.9 wt%Pb alloy.

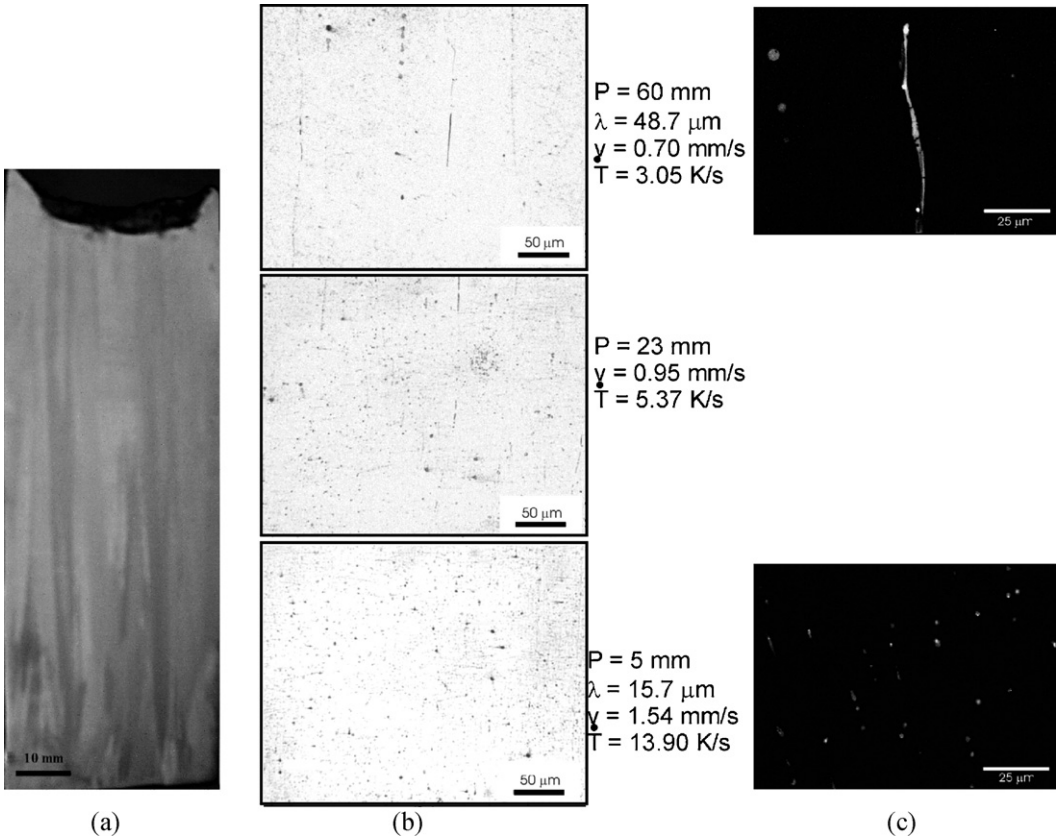

Fig. 6. (a) Directionally solidified macrostructure; (b) longitudinal microstructures and (c) microstructural details of the Pb-rich droplets and fibers (SEM images) of the Al–1.2 wt%Pb alloy.

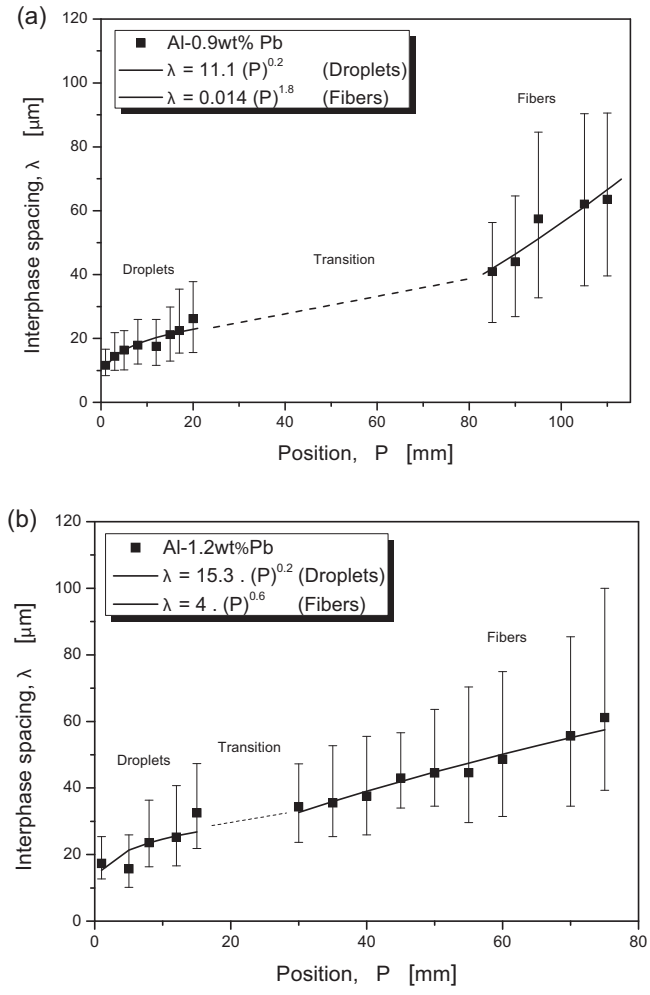

Fig. 7. Interphase spacing as a function of position along the casting length for (a) Al–0.9 wt%Pb and (b) Al–1.2 wt%Pb alloys.

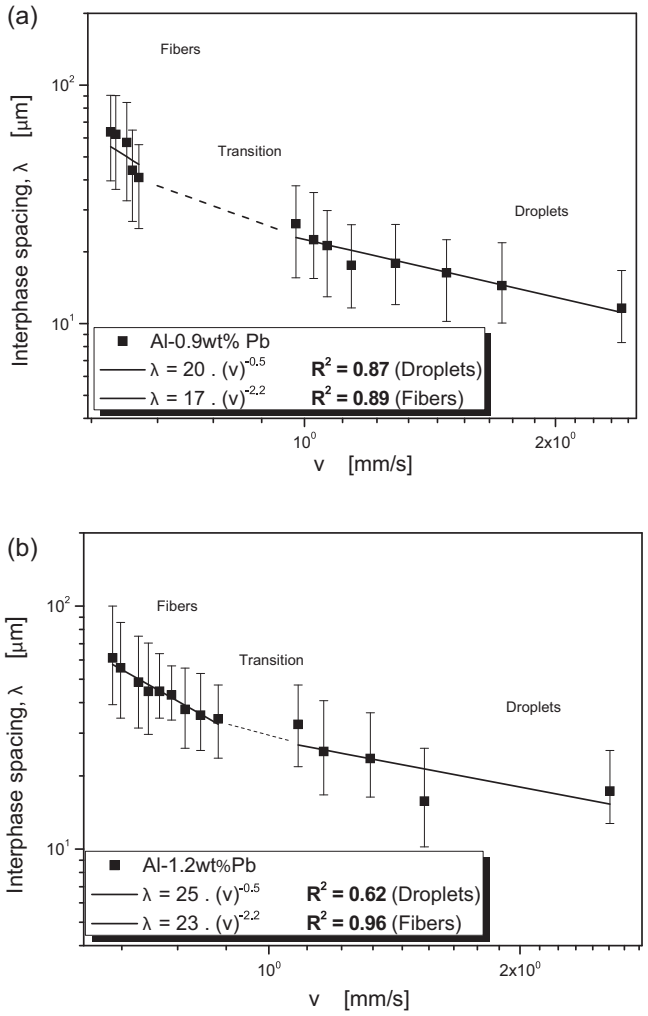

Fig. 8. Interphase spacing of droplets and fibers as a function of the growth rate for (a) Al–0.9 wt%Pb and (b) Al–1.2 wt%Pb alloys. R^2 is the correlation coefficient.

in recent studies concerning the transient solidification of Al–Bi monotectic alloys [23–25]. The range of maximum and minimum experimental diameters that can be observed for a same position in casting seems to be related to the typical thermal instabilities of the solidification front, which is a consequence of the transient regime of heat extraction.

The functional dependence of the interphase spacing during monotectic growth can also be established as a function of the product Gv [26], as shown in Fig. 10 for both fibrous and droplets morphologies from the present study. The same exponents for G and v were experimentally defined for both alloys, $-1/4$ and $-1/8$, respectively, and are the same proposed in theoretical models of dendritic growth [27–29]. These same exponents were also experimentally found to be appropriate to represent the experimental evolution of interphase spacings for a monotectic Al–3.2 wt%Bi alloy solidified under unsteady-state conditions [23].

An appropriate design of the final monotectic structure can be critical considering particular industrial applications. For instance fibrous structures are desired for the fabrication of porous aluminum with deep pores by using electrochemical etching [30,31]. This material can be applied to filters or heat exchangers. Al–Pb monotectic alloys are especially attractive as self-lubricating bearing alloys if the soft Pb-rich phase could be well-dispersed in the solid microstructure [5]. Thus, the control of the solidification process by the pre-programming of solidification processing variables based on experimental growth laws such as those proposed in the present study, can be used as an alternative way to produce components of monotectic alloys having microstructural arrangements, which are conducive to specific applications.

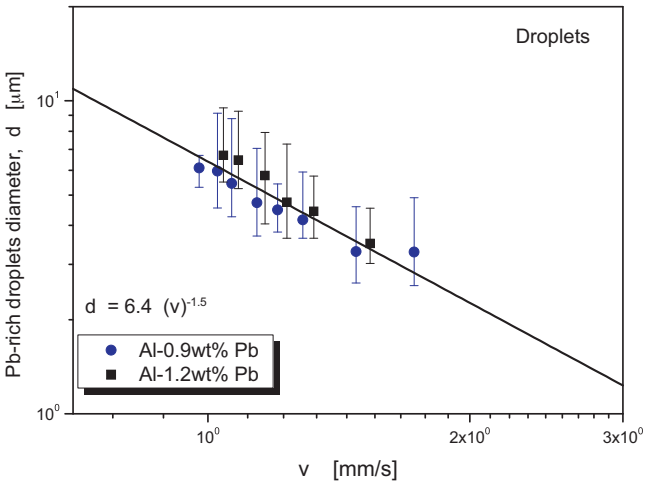

Fig. 9. Diameter of Pb-rich droplets as a function of the growth rate.

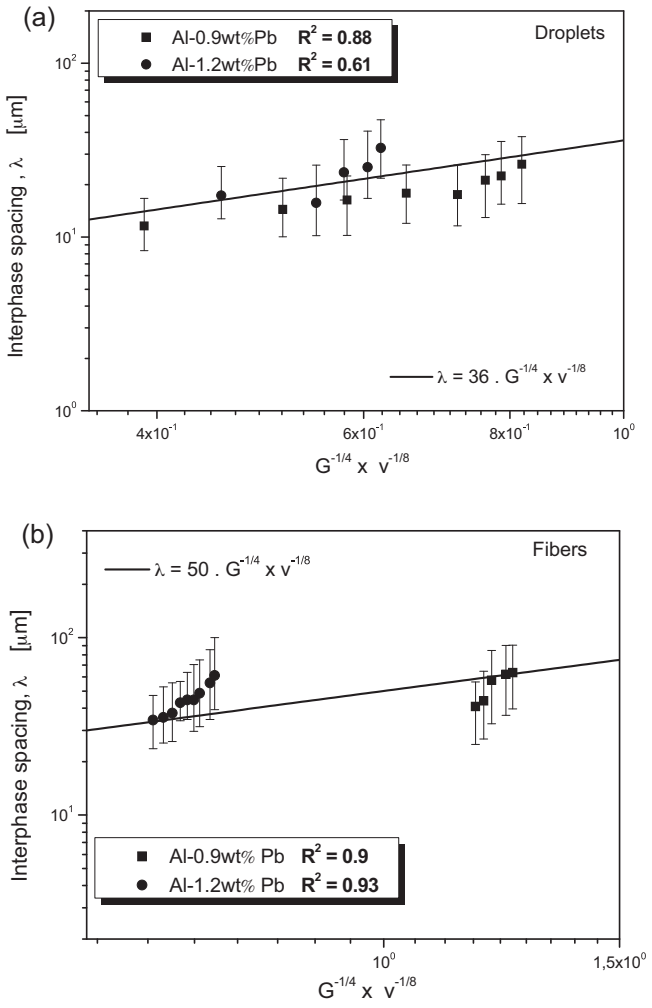

Fig. 10. Interphase spacing as a function of $G^{-1/4} \times v^{-1/8}$ for (a) droplets and (b) fiber-like morphologies.

4. Conclusions

The following major conclusions can be drawn from the present study:

- The microstructures of the Al–0.9 wt%Pb and Al–1.2 wt%Pb alloys are formed by well-dispersed Pb-rich droplets in the aluminum-rich matrix for $v > 1.0$ mm/s and $v > 1.1$ mm/s, respectively. On the other hand, a fiber-like Pb-rich phase and string of pearls prevail for $v < 0.65$ mm/s and $v < 0.87$ mm/s for Al–0.9 wt%Pb and Al–1.2 wt%Pb alloys, respectively. The range of growth rates between these limiting values is associated with a region of morphological transition characterized by the coexistence of Pb-rich fibers and droplets distributed in the Al-rich matrix.
- Two different experimental power laws with exponents −2.2 and −0.5 expressing λ as a function of v were found to better represent the monotectic growth of both Al–Pb alloys examined for fibrous and droplets morphologies, respectively. The functional dependence of the interphase spacing during monotectic growth has also been experimentally established as a function of the product Gv.
- An average constant C of about 5.5×10^{-13} was found to fit the classical growth law $\lambda^2 v = C$ for the growth of Pb-rich droplets for both alloys examined in the present study.

Acknowledgements

The authors acknowledge the financial support provided by FAPESP (The Scientific Research Foundation of the State of São Paulo, Brazil), CNPq (The Brazilian Research Council) and FAEPEX-UNICAMP.

References

[1] B. Predel, L. Ratke, H. Fredriksson, in: H.U. Walter (Ed.), Fluid Sciences and Materials Science in Space, Springer-Verlag, Berlin, 1987, pp. 517–565.
[2] H. Neumann, Y. Plevachuk, F. Allenstein, Mater. Sci. Eng. A 361 (2003) 155–164.
[3] J.Z. Zhao, S. Drees, L. Ratke, Mater. Sci. Eng. A 282 (2000) 262–269.
[4] G. Ran, J. Zhou, S. Xi, P. Li, J. Alloys Compd. 419 (2006) 66–70.
[5] J. An, X.X. Shen, Y. Lu, Y.B. Liu, Wear 261 (2006) 208–215.
[6] E. Johnson, A. Johansen, U. Dahmen, S. Chen, T. Fujii, Mater. Sci. Eng. A 304–306 (2001) 187–193.
[7] J.Z. Zhao, Scripta Mater. 54 (2006) 247–250.
[8] Parr et al., Preparation of monotectic alloys having a controlled microstructure by directional solidification under dopant-induced interface breakdown, US patent no. 4198232, 1980.
[9] Y.C. Suh, Z.H. Lee, Scripta Metall. Mater. 33 (1995) 1231–1237.
[10] H. Li, J. Zhao, Comput. Mater. Sci. 46 (2009) 1069–1075.
[11] L. Ratke, Adv. Space Res. 16 (1995) 95–99.
[12] L. Ratke, Mater. Sci. Eng. A 203 (1995) 399–407.
[13] S. Ozawa, T. Motegi, Mater. Lett. 58 (2004) 2548–2552.
[14] W.F. Kaukler, F. Rosenberger, P.A. Curreri, Metall. Mater. Trans. A 28 (1997) 1705–1710.
[15] L. Ratke, A. Müller, Scripta Mater. 54 (2006) 1217–1220.
[16] L. Ratke, Mater. Sci. Eng. A 413–414 (2005) 504–508.
[17] K.A. Jackson, J.D. Hunt, Trans. Metall. Soc. AIME 236 (1966) 1129.
[18] B. Derby, J.J. Favier, Acta Metall. 31 (1983) 1123–1130.
[19] R.N. Grugel, A. Hellawell, Metall. Trans. A 12 (1981) 669–681.
[20] S. Yang, W. Liu, J. Mater. Sci. 36 (2001) 5351–5355.
[21] R.N. Grugel, T.A. Lograsso, A. Hellawell, Metall. Trans. A 15 (1984) 1003–1012.
[22] G. Lang, Aluminium 48 (1972) 664–672.
[23] A.P. Silva, J.E. Spinelli, A. Garcia, J. Alloys Compd. 475 (2009) 347–351.
[24] A.P. Silva, J.E. Spinelli, A. Garcia, J. Alloys Compd. 480 (2009) 485–493.
[25] A.P. Silva, J.E. Spinelli, N. Mangelinck-Nöel, A. Garcia, Mater. Des. 31 (2010) 4584–4591.
[26] T. Carlberg, A. Bergman, Scripta Metall. 19 (1985) 333–336.
[27] J.D. Hunt, International Conference on Solidification and Casting of Metals, The Metals Society, London, 1979, pp. 3–9.
[28] W. Kurz, J.D. Fisher, Acta Metall. 29 (1981) 11–20.
[29] R. Trivedi, Metall. Mater. Trans. A 15 (1984) 977–982.
[30] H. Yasuda, I. Ohnaka, S. Fujimoto, N. Takezawa, A. Tsuchiyama, T. Nakano, K. Uesugi, Scripta Mater. 54 (2006) 527–532.
[31] H. Yasuda, I. Ohnaka, S. Fujimoto, A. Sugiyama, Y. Hayashi, M. Yamamoto, A. Tsuchiyama, T. Nakano, K. Uesugi, K. Kishio, Mater. Lett. 58 (2004) 911–915.